TEXRAY: Textile Identification via Raman Spectroscopy

Ariana Mihandoost, Danielle Samuels, Austin Frost, Cameron Ricketts

Dept. of Electrical Engineering and Computer Science and Dept. of Optics and Photonics, University of Central Florida, Orlando, Florida, 32816-2450

***Abstract* — TEXRAY is a lightweight, portable system designed to help users quickly and accurately verify the composition of textiles and fabrics via Raman spectroscopy. Raman scattering is an optical phenomenon in which light scattered off of a material has a different frequency than the incident light, with these shifts corresponding to molecular bonds and vibrational modes within the material. This leads to a unique Raman "fingerprint" for every substance, useful for identification. TEXRAY leverages this principle to allow users to distinguish between common textile types, such as cotton and polyester samples, offering a reliable method for the verification of clothing composition.**

***Index Terms* — Raman spectroscopy, Raman scattering, laser diodes, charged-coupled devices, photonics, optics**

I. INTRODUCTION

TEX-RAY is a consumer-minded product utilizing the concept of Raman scattering to identify the composition of a textile or fabric. Many modern consumers are prioritizing purchasing natural fibers only, some for environmental reasons, such as reducing microplastic pollution, and others for comfort or health concerns. This growth in the natural fiber market has led to a parallel increase in merchants misleading shoppers about the fabrics comprising their products, hoping to capitalize on market trends. The average shopper has few means of verifying whether or not the label on their clothes is accurate, and can easily fall susceptible to retailers' deception. TEXRAY aims to target this issue and allow consumers to quickly and easily verify whether their fabrics are natural or synthetic.

Raman scattering is a phenomenon that happens to 1 in 10 million photons. It occurs when the electromagnetic field of a photon incident on a molecule excites the molecule's electrons to an unstable virtual state. These electrons immediately relax to a different energy level, causing a photon to be re-emitted at a different wavelength than the incident light. This project focuses on Stokes scattering, in which the electron relaxes down to a higher energy level than the initial ground state, releasing a photon at a lower energy and thus higher wavelength than the incident photon. Stokes shift occurs at wavelengths unique to the material the light is scattering off, creating a fingerprint spectrum that can be used to identify substances based on their characteristic Raman spectrum.

TEXRAY utilizes this fingerprint to determine whether a sample is comprised of cotton or polyester. The user will place their unblended fabric in a designated location and select one of two system modes on the LCD screen: “Material Analysis” or “Product Comparison.” Material analysis will analyze the Raman spectrum of the present sample and determine whether the collected spectrum is characteristic of polyester or cotton, then read the result out to the user via the LCD screen. In contrast, product comparison, will allow the user to scan any blended fabric or clothing item to acquire its characteristic spectrum. If the product’s spectrum matches a previously stored scan, then the LCD screen will display the matched product name to the user. If no similar entry exists in the system, the user will be prompted to add a label for the new item’s scan.

II. KEY SPECIFICATIONS

The engineering requirements of our system specify a 90% accuracy in differentiating between a cotton and polyester sample, 90% accuracy in a general textile product comparison, and to hold a system processing time of 15 seconds from initiation to completion.

II. SYSTEM COMPONENTS

The following section briefly details the major components integrated into TEX-RAY.

A. Laser

A 532 nm laser was chosen for our system due to this wavelength’s balance between Raman scattering efficiency and minimization of fluorescence. As Raman scattering is proportional to λ^{-4}, lower wavelengths generate the most distinguishable Raman signal [1]. This wavelength was also tested with our samples of interest, cotton and polyester, and was shown to produce minimal fluorescence, making it easier to recover their characteristic Raman peaks. Additionally, because 532 nm light is in the visible range, it is more convenient for ensuring system alignment compared to a UV laser, which many Raman spectrometers employ. Our selected laser is the Q-BAIHE laser module, as it comes conveniently packaged with an accompanying laser driver board and collimating lens. Additionally, the

spectral linewidth of this laser is approximately 1 nm, which will provide high spectral resolution for our system.

B. Dichroic mirror

Our Raman system utilizes a dichroic mirror rather than a traditional beamsplitter to minimizes laser power loss onto the sample as well as Raman signal loss upon collection. The dichroic mirror will selectively reflect the laser line towards the sample such that it can be focused into a tight spot by a planoconvex lens. The resulting Raman scattering that is collected by this lens will then be allowed to transit back through the dichroic mirror. The dichroic mirror we selected is the Chroma T550lpxr, due to its high transmittance and reflectance of 96% and 97%, respectively. This ensures that almost all of the laser's power is incident on the sample, maximizing Raman signal generation, and that almost all of this signal can pass back through the system, maximizing Raman signal collection.

C. Longpass filter

The longpass filter is a pivotal component in any Raman system. Because Raman scattering only affects one in every ten million photons, it can easily be drowned out by any excess laser light or Rayleigh scattering hitting the detector. A longpass filter of high optical density should be implemented to block all wavelengths at and below the laser line, ensuring that only the Raman scattered photons are hitting the detector surface. The filter chosen for our system is the Chroma ET542lp. This filter has OD6 blocking up until 539 nm, and a transmittance of 98%, ensuring that all laser line and Rayleigh scattering is eliminated and that minimal Raman signal is lost upon passing through the optic.

D. Diffraction Grating

The selected dispersive component of the system is the GR25-1205 ruled, reflective diffraction grating. This grating, blazed at 500 nm, was chosen for its high diffraction efficiency around our desired wavelength range. Holographic and transmissive gratings comparatively reduce stray light, however, display lower efficiencies. The ruled, reflective design is more suited for maximizing signal collection, is particularly important to account for the low intensity Raman signals. The1200 grooves/mm groove density was chosen to allow for high angular dispersion, which allowing prompts the high resolution needed to differentiate between the closely spaced wavelengths within a Raman spectrum. While a higher groove density reduces the dispersed spectral range, this is acceptable as we are only interested in a 90 nm range.

E. Charged-Couple Device (CCD)

The linear array CCD integrated into the spectrometer serves the critical role in detecting the low intensity Raman signal. A CCD was chosen over a CMOS sensor for its better suitability in low-light conditions. The chosen CCD, the Toshiba TCD1304DG, is a widely adopted linear CCD for spectroscopy applications. Its various specifications make it suitable for detection in TEX-RAY. The 29.1 mm detector width comfortably accommodates our desired 90 nm spectral range, and the 8 μm pixel width—paired with a 25 μm entrance slit of the spectrometer, enables a sufficient theoretical resolution. Further, the spectral sensitivity of approximately 100% aligns with our desired spectral range. The dynamic range of 300:1 enables us to differentiate signals with significantly varying intensities. With a clock frequency of 2MHz to drive the CCD, the output is captured at a rate of 500kHz, this quick data rate helps minimize our system's total response time.

F. Textile Samples

For material classification, TEXRAY is tested on unblended, undyed textile samples to avoid interference from dyes and additives, which can degrade Raman signal and introduce fluorescence. We used standardized fabrics from Test Fabrics, Inc, specifically ISO adjacent cotton and polyester, to provide a reliable spectral baseline and improve accuracy. The product comparison feature supports any household textiles, including dyes and blends.

G. Optical Component Assembly

The CAD design of the optical component housing for our system plays a significant role in reducing the cost and size of TEXRAY while maintaining quality optical performance. Since sensitive alignment dictates the efficiency of our system, particular attention was paid to the tolerancing and design constraints during the modeling process. All components were designed using Onshape.

H. Hosyond Five-Inch Liquid Crystal Touchscreen Display

The spectral signature of the current sample, all user input, and results of material sorting and product identification are all shown through the Hosyond five-inch liquid crystal touchscreen display. The display is powered by and attached directly to the Raspberry Pi through a Display Serial Interface ribbon cable. From the display, the user can select the system setting and initiate the CCD data acquisition, the results of which are displayed to the user on the display along with the identified material or product the sample was matched with, depending on the system setting that was selected.

I. Power Supply

For TEXRAY, a DC battery power supply was chosen over solar and AC options due to its reliability, stability, and portability—key requirements for a mobile spectrometer. Solar power, while renewable, is less reliable in varying environmental conditions and requires more space and cost. AC power, though stable, lacks portability and depends on external infrastructure.

Among battery types, Lithium-ion offers high energy density, but raises safety concerns. SLA batteries are cheaper but too bulky and short-lived for portable use. Lithium Iron Phosphate ($LiFePO_4$) provided the best balance of safety, lifespan, and performance, making it the ideal choice.

To ensure safety and ease of integration, the Nastima 12V 6000mAh $LiFePO_4$ battery pack was selected. Although it provides 12V, 9V, and 5.2V outputs, the 9V line was used for its better voltage stability. The pack includes built-in protection features, removing the need for external charging circuits and supporting the project's focus on portability, reliability, and simplicity.

J. ESP32-WROOM-32D

The system's main printed circuit board, which controls the flow of power to the laser module and Raspberry Pi, is operated using an ESP32 microcontroller unit. The MCU is programmed using the Arduino development environment and the CP2102 programmer.

K. STM32F401CCU6

The CCD sensor is driven and sampled by the STM32F401CCU6 microcontroller unit, with the sensor's output signal voltage obtained and converted into raw binary data before being sent to the Raspberry Pi. The printed circuit board on which the MCU lies is an exact replication of the STM32F401CCU6's "black pill" model development board. The MCU is programmed using the STM-32 Cube development environment and the ST-Link V2, an in-circuit debugger and programmer device designed for the STM-8 and STM-32 microcontrollers. The MCU is powered through a USB-C cable connection between the STM-32 development board PCB and the Raspberry Pi.

L. Raspberry Pi 5

The liquid crystal display, system startup initiation, comparison algorithm, material classification, and product matching are all run using the Raspberry Pi 5 single-board computer. The Raspberry Pi in our system runs on the standard Raspbian operating system developed by Raspberry Pi Holdings, the same company that develops the Raspberry Pi. The system code running on the Raspberry Pi is written in Python.

III. System Operation

This section will describe how the prior components function together to provide the user with the spectral analysis results.

A. Probe Optics

Once the laser is turned on by the user selecting a TEXRAY operating mode, the laser light will be directed into a f = -6 mm planoconcave lens to diverge the 1 mm diameter laser beam. Following this lens at a distance of 94 mm, a f = 100 mm planoconvex lens will re-collimate the laser light to a spot size of approximately 16 mm. The dichroic mirror will be place at a 45° angle to the incoming laser light, reflecting it onto a f = 18 mm planoconvex focusing lens which will concentrate the laser line onto the sample, generating Raman scattering. This light, which is scattered in all directions, will be re-collimating by the focusing lens and directed back through the dichroic mirror and the subsequent longpass filter, which will eliminate any remaining laser light and Rayleigh scattering. Finally, a f = 75 mm planoconvex lens will focus the Raman signal and couple it to the spectrometer entrance slit. This configuration is shown more clearly in fig. 1.

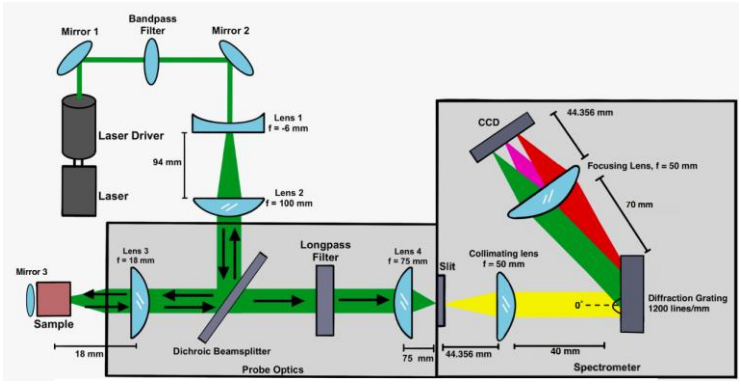

Fig. 1. Layout of all optical components in the system.

B. Spectrometer

The spectrometer portion of TEX-RAY is responsible for separating the Raman scattered light into its constituent wavelength components. The spectrometer portion is designed to accept a wavelength range of 550 nm to 640 nm, which corresponds to the range of shifted wavelengths that contains identifying peaks for cotton and polyester. We're looking to achieve a spectral resolution of less than or equal to 1 nm to thoroughly differentiate cotton and polyester spectra as well as conduct a reliable product comparison.

The slit of the spectrometer acts as a spatial filter and controls the amount of light introduced into the system. The light diverging out of the slit then gets collimated by 50 mm achromatic lens, this collimated beam is incident onto the reflective diffraction grating. The diffraction grating will separate the Raman signal into its wavelength components. These separated wavelengths will then be focused on the linear array CCD by another 50 mm achromatic lens.

C. Software

All user interaction with the system is received through the liquid crystal display, which is connected directly to the Raspberry Pi. The system's startup begins with the selection of a system setting on the display, choosing between options of "Material Analysis" and "Product Comparison." Once the decision is made, the Raspberry Pi communicates with the ESP32 on the main printed circuit board to begin supplying voltage to the laser module so that the spectrum of the current sample can be obtained. Communication between the ESP32 MCU and the Raspberry Pi is set up using UART, with the ESP32 setting a general-purpose input/output pin to high in connection with a transistor when a simple message of '1' is received from the Raspberry Pi. Once the command is sent, the laser module will begin operating, and at the other end of the optics subsystem, the spectrum of the current sample will be projected onto the TCD1304DG CCD sensor.

The CCD is driven by the STM32 microcontroller using three input signals. These three signals, the shift-gate, master-clock, and clear-gate, coordinate the timing of the output signal from the CCD, ensuring the data of each pixel on the sensor is sent. The fourth signal on the STM32 is internal, coordinating the operation of the embedded analog-to-digital converter that samples the analog output voltage signal from the CCD and converts it into raw binary data. This data is transmitted from the STM32 to the Raspberry Pi through the USB-C cable that also powers the STM32.

The cable sends binary data back to the Raspberry Pi after a pre-set period has passed from when the original UART command was sent to the ESP32. This raw binary data is automatically taken and stored in the "/dev/ttyACM0" file on the Raspberry Pi. The VCP used for the data transfer is then disconnected, and the file is loaded into the running Raspberry Pi Python code.

The file's contents are converted into integer data, and the data of a singular frame is taken to be used in the comparison algorithm. The frame of data is first subjected to noise reduction and calibration processes. A Savitzky-Golay filter is used to create a baseline of fluorescence and noise present in the data by separating the frame into a series of consecutive sections and fitting each section using a low-degree polynomial function. The baseline is formed by combining the polynomial fit of each section into one complete function; the values from this function are subtracted from the original dataset to produce a new noise-reduced dataset suitable for comparison. The noise-reduced data is also calibrated along its x-axis using the results of trials run with spectra containing visible peaks at known wavelengths. At the end of these processes, the resulting data becomes the test data used for comparison calculations. Before these comparisons are made, though, the noise-reduced spectral signature data is first displayed to the user as a line graph on the same LCD that was used to initiate the system's startup.

The system's comparison algorithm is built around the time-series analysis method known as dynamic time warping. In this method, two line graphs are compared using a selected distance metric; in our project, Euclidean distance is used. The unique aspect of dynamic time warping, however, is that the effect of a data point's placement along one axis, usually the x-axis in time-series analysis, is intentionally limited. This is done by calculating the Euclidean distance between points lying on different graphs using points of comparison rather than matching them by a common x-coordinate. The rules in determining points of comparison are that every point in both line graphs must be matched with at least one point of comparison in the other graph, and the sequence of matching cannot go backward, meaning that if you imagine every point of comparison as a line stretching from a point in one graph to a point in the other, then these lines cannot cross over one another (fig. 2). To identify each point of comparison, a cost matrix is calculated, using the Euclidean distance between the current point in the first line graph and all available points in the second line graph as the index values of the cost matrix. Paths through the matrix are simulated and compared using the sum of every index value used in the path. The smallest sum possible through the matrix becomes the similarity score of the two line graphs, which is the final result of the dynamic time warping comparison.

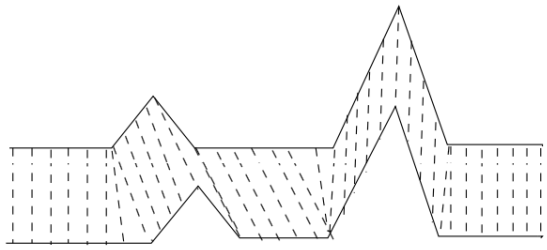

Fig. 2. Visual representation of points of comparison in Dynamic Time Warping [2].

This similarity score is used to classify the spectral data of the system's current sample. In the case of the "Material Analysis" setting, this is done using k-Nearest Neighbors classification. The textile sample's spectral data is compared against the stored data from previous textile system trials. The similarity score calculated for each prior trial is labeled with the material of the sample from the corresponding trial. These scores are analyzed, with the K smallest scores being used to sort the current sample. In the case of dynamic time warping, the smaller the similarity score, the more similar the two line graphs are. The labels of each of the K smallest scores are grouped together, and the label most represented within the group is the material the current sample is sorted into. This label is displayed to the user as the identified material of the sample on the LCD. The identification process is similar but slightly different in the case of the "Product Comparison" setting. The spectral signature data of the current sample is, in this case, compared with the data of previous clothing item trials, and the comparison results are tested against a similarity threshold rather than the k-Nearest Neighbors algorithm. If the current sample's data produces a similarity score with a prior scan that lies under the similarity threshold, then the item label of the matched trial is displayed to the user as the identified product of the current sample. If no similarity score passes the threshold, then the user is prompted to input a title for the new product, and the title is then stored as the ID label for the item. In both instances, the LCD is used to display the final result of the system (fig. 3).

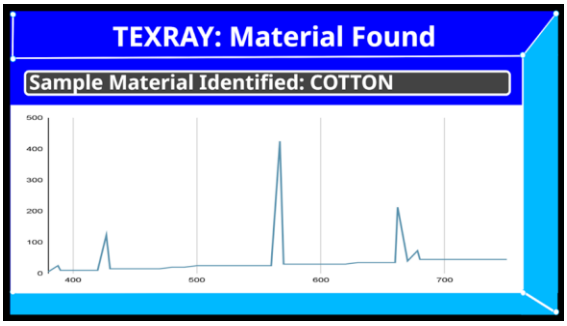

Fig. 3. Diagram of User Interface on the Liquid Crystal Display Showing Final Results of "Material Analysis" Setting.

IV. Hardware Design

Many different considerations went into the layout and system operations as described in the previous section, which will be explained here.

A. Probe optics beam expander

To select the lenses utilized in the beam expander segment, multiple factors came into play. Initially, the f = 18 mm focusing lens utilized in the probe optics was chosen assuming a laser beam diameter of approximately 3 mm. Aiming for a focused spot size of 5 µm, (1) was used, where f is the focal length of the lens, ω_0 is the beam waist at the sample, D is the collimated beam diameter at the focusing lens, and M^2 is the beam quality parameter, which quantifies how far the beam diverges from an ideal Gaussian beam [3].

$$f = \frac{2(2.5\ \mu m)\pi(3\ mm)}{4(1.2)(532\ nm)} = 18.45\ mm \qquad (1)$$

However, after receiving our laser, the beam turned out to be closer to 1 mm in diameter rather than 3 mm, resulting in a focused spot size of approximately 14 µm. Zemax simulations showed a similar expected result of 12 µm. Though this value is technically acceptable, as Raman spectroscopy demands a focused spot of between 10-20 µm, we were not able to get any Raman peaks to appear through testing with this set up, leading us to implement a beam expander. Expanding the beam to a larger diameter will enable a tighter focus at the sample assuming the same focusing lens, according to (1).

Because our smallest probe optic has a diameter of 18 mm, we chose to expand our beam to as close to 18 mm as possible, keeping distance restrictions in mind. Using a simple Galilean beam expander design, a f = -6 mm plano-concave lens and a f = 100 mm aspheric lens were chosen, as we already had the aspheric lens handy. In a Galilean beam expander, the distance between optics is equal to the difference between their focal lengths, or in our case, 94 mm. As shown in fig. 5, Zemax simulations confirmed this lens configuration would result in a 16 mm expanded beam diameter.

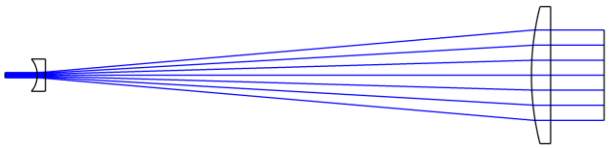

	Surface Type		Comment	Radius	Thickness		Material		Clear Semi-Dia	
0	OBJECT	Standard		Infini...	Infinity				0.000	
1		Standard		Infini...	5.990				0.500	
2	STOP (aper)	Standard	LC2969	-4.670	1.500		N-SF...		3.000	U
3	(aper)	Standard		Infini...	0.000				3.000	U
4		Standard		Infini...	90.721	V			0.573	
5	(aper)	Standard	LA1509	51.500	3.590		N-BK7		12.700	U
6	(aper)	Standard		Infini...	0.000				12.700	U
7		Standard		Infini...	10.000				8.403	
8	IMAGE	Standard		Infini...	-				8.391	

Fig. 5. Zemax simulation of Galilean system. Clear Semi-Dia of the system after the beam expander is 8.403, indicating an expanded beam diameter of 16.806 mm.

B. Spectrometer

The design of the spectrometer was an iterative process which dictated the component configuration that would allow us to meet our spectral resolution and range requirement. A lens-grating-lens (LGL) spectrometer configuration consisting of a collimating lens, reflective diffraction grating, and focusing lens was ultimately chosen for its compactness, alignment ease, and high throughput. We moved forward with a symmetrical system, where both the collimating and focusing lens have matching 50 mm focal lengths [4].

The final component of the probe optics portion is a 75 mm condenser lens that focuses an 18 mm beam onto the entrance slit of the spectrometer, resulting in an f/# of 4.16. The f/# of the spectrometer, determined by the 50 mm collimating lens divided by the consequent theoretical 12 mm beam diameter, was intentionally matched to this f/# value to maximize light throughput in the system.

The entrance slit of the spectrometer is a critical parameter which dictates the resolution and the light throughput of the system. Where the wider the slit the more light collected yet the spectral resolution decreases. This is especially relevant considering the low power nature of the Raman signal. According to the Nyquist criterion, to sample a spectral feature, the slit image must span 2-3 pixels. Given the 8 µm pixel size on the CCD, the a 25 µm slit sufficiently spans ~3 pixels.

After considering proper coupling of the Raman signal into the spectrometer, we determined the ideal incident and diffraction angle pair to efficiently disperse the Raman signal onto the detector. The diffraction grating equation, (3), can be rearranged to solve for the diffraction angle β, given a groove spacing d, center wavelength of 595 nm, and +1 mode order m.

$$m\lambda = d\,(sin\alpha + sin\beta) \tag{2}$$

Although operating at the Littrow configuration (α = β) maximizes grating efficiency, it also diffracts the first order beam back towards the input path, making it impossible to detect. To avoid this overlap while maintaining a reasonable efficiency, an incident angle of 10° was chosen which results in a diffracted angle of 32.5°.

The diffraction angles directly influence the spectrometer's dispersion characteristics.

$$\frac{d\lambda}{dx} = \frac{d * cos\beta}{m * F_f} \tag{3}$$

$$d\lambda = \frac{d\lambda}{dx} * W_s \tag{4}$$

$$spectral\ range = \frac{d\lambda}{dx} * W_d \tag{5}$$

Using (4), the reciprocal linear dispersion is calculated as 14.024 nm/mm, which describes the wavelength dispersion per unit length. We can further use the reciprocal linear dispersion paired with a 25 µm slit width, W_s, in (5) to determine the theoretical spectral resolution of the system as 0.351 nm. Additionally, the reciprocal linear dispersion paired with a 29.1 mm detector width, W_d, in (5) to determine the theoretical spectral range receivable by the detector results in a receivable wavelength span of 408 nm. Which more than compensates for our desired 90 nm span. Zemax was used to corroborate our design choices and guide the selection of lenses for the spectrometer. Achromatic lenses were ultimately chosen for their ability to minimize chromatic aberrations. Optimizations were performed to minimize aberrations and improve spot quality, resulting in the lens distances as seen in fig. 1.

C. Voltage Regulators

The voltage from the battery will be fed into voltage regulators once powered on. This is necessary to ensure a constant voltage supply throughout the system while providing the specific voltages each component requires. For this, switching voltage regulators were chosen due to their high power efficiency and ability to either step voltage up or down as needed. Linear regulators, while simpler, were avoided due to their tendency to waste energy as heat, which would reduce overall system efficiency and require additional cooling.

To properly supply the components within the system, 3.3V, 5V, and 12V outputs were needed. A boost converter,

the LM2587S, was used to step the 9V battery output up to 12V for components requiring higher voltage. For stepping down to 5V and 3.3V, buck converters were used, specifically, the LM22679 for 5V and the LM2576 for 3.3V. This configuration allows the TEXRAY system to efficiently distribute power to all modules while maintaining voltage stability, which is especially important for sensitive electronics like the CCD and STM32 microcontroller.

E. 3.3 Volt Regulator Schematic

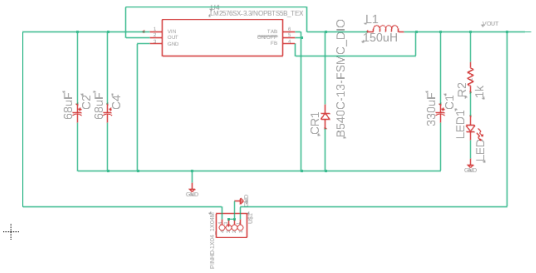

Fig. 7. Voltage Regulator 3.3 Schematic

This schematic shows the 3.3V regulator used in the system. The LM2576 steps the 9V input down to 3.3V and provides up to 1A of current. Both the input and output are routed through a four-pin header so the regulator can be placed on a daughter board separate from the main board. From there, the 3.3V line connects to the components that require it. An LED is added to the output to show when the circuit is active and voltage is present.

F. 5.2 Volt Regulator Schematic

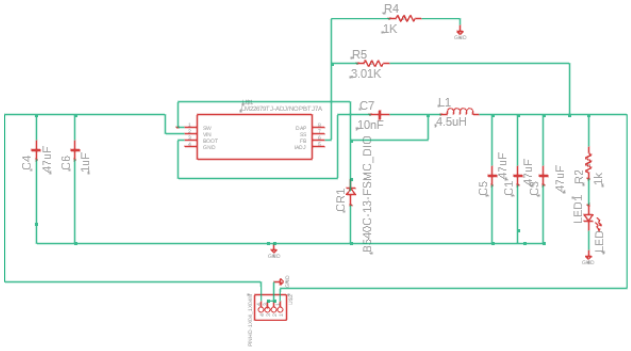

Fig. 8. Voltage Regulator 5.2 Schematic

This is the schematic for the 5.2V regulator daughter board. Like the previous one, it steps down the 9V input, but this time using the LM22679 adjustable version. The output voltage is set by the 1kΩ (R4) and 3.01kΩ (R5) resistors based on the regulator's internal reference voltage, as seen in formula (6). This circuit is designed to supply 5.2 V at up to 5A to meet the needs of its load. An LED is also included to indicate when power is being delivered.

$$V_{OUT} = V_{REF} * \left(1 + \frac{R_5}{R_4}\right) \quad (6)$$

G. 12 Volt Regulator Schematic

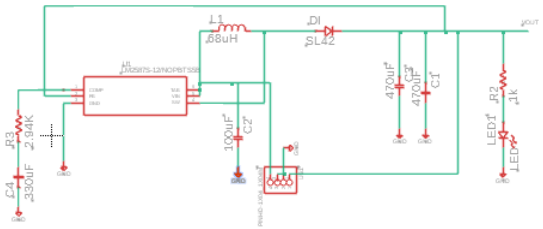

Fig. 9. Volt Regulator 12 Schematic

As mentioned earlier, the LM2587S is used as the boost converter to step the 9V input up to 12V. This regulator is placed on a daughter board and is set up to output 1A to the components on the main board. Like the other regulator boards, it includes an LED to indicate when 12V is being supplied.

H. Main Board Schematic

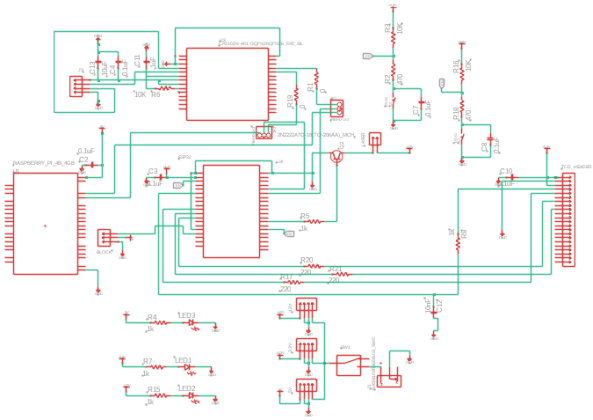

Fig. 10. Main Board Schematic

This schematic shows how the components on the main board are connected. The board is responsible for holding the regulators and the main components: the ESP32, Raspberry Pi 5, laser, and CP2102. The laser is controlled by the ESP32, which receives input from the Raspberry Pi through its connected LCD. The CP2102 serves as a USB-to-UART bridge to program the ESP32. The 3.3V regulator powers the ESP32, the 5.2V output goes to the Raspberry Pi 5, and the 12V line supplies power to the laser. Each power rail includes an LED to indicate when voltage is present and the system is active.

I. STM32 Schematic

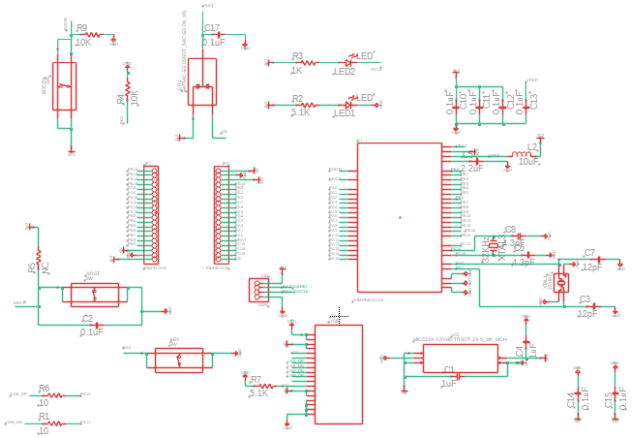

Fig. 11. STM32 Black Pill Schematic

Above is the STM32 schematic, which is based on the design of the STM32 Black Pill development board. This board will be mounted on the CCD board and connected to the Raspberry Pi 5 through a USB-C connection. The STM32 is responsible for analyzing the incoming signal from the spectrometer.

J. Signal Analysis Board Schematic

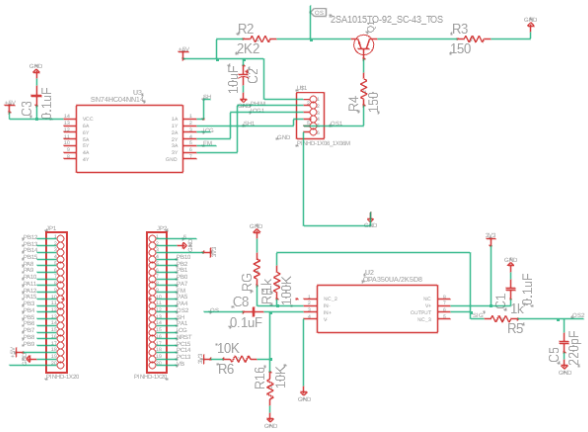

Fig. 12. Signal Analysis

This board is responsible for analyzing the signal coming from the CCD. The two 20-pin headers represent the STM32 board's pin layout. The CCD's master clock, integration clear gate, and sample-and-hold signals are routed through a SN74HC04N hex inverter and then connected to STM32 pins A6, A0, and A2. The OPA350 op-amp is used to amplify the CCD's analog output, as the signal is initially very low. Once amplified, the signal passes through a low-pass RC filter to reduce noise before being read by the STM32's ADC pin.

K. TCD1304DG Board Schematic

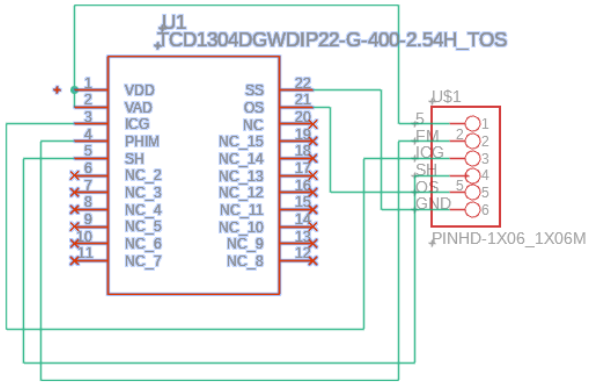

Fig. 13. TCD1304DG Board Schematic

The purpose of this board is to house the TCD1304DG CCD sensor and provide secure connections to the signal analysis board through the header and receive its input voltage from the 5V pin on the STM32. This setup allows the CCD to be properly positioned and angled without being restricted by the size or layout of the larger boards.

V. Conclusion

This project has been an interdisciplinary feat of creating a Raman spectrometer prototype that allows one to conduct textile product authentication in an affordable and reliable way.

VI. Acknowledgements

Special thanks to our sponsors, Chroma and Test Fabrics, Inc. We'd also like to extend our gratitude towards the CREOL community.

VII. References

[1] D. Tuschel, "Selecting an Excitation Wavelength for Raman Spectroscopy," vol. 31, pp. 14–23, Mar. 2016.
[2] *Dynamic Time Warping*. (2015, July 15). Wikipedia. https://commons.wikimedia.org/wiki/File:Dynamic_time_warping.png
[3] OphirBlog, "How to Calculate Laser Beam Size," Ophir Photonics. Accessed: Mar. 29, 2025. [Online]. Available: https://blog.ophiropt.com/calculate-laser-beam-size/
[4] "Raman Spectroscopy for Chemical Analysis | Wiley Online Books." Accessed: Apr. 22, 2025. [Online]. Available: https://onlinelibrary.wiley.com/doi/book/10.1002/0471721646